

## FIELD EMISSION MEASURE DURING CERL MAIN LINAC CRYMODULE HIGH POWER TEST IN KEK

Enrico Cenni<sup>#</sup>, The Graduate University for Advanced Studies, KEK, Tsukuba, Ibaraki, Japan  
 Kazuhiro Enami, Takaaki Furuya, Hiroshi Sakai, Masato Satoh, Kenji Shinoe, Kensei Umemori  
 KEK, Tsukuba, Ibaraki, Japan  
 Masaru Sawamura, JAEA, Tokai, Naka, Ibaraki, Japan

### Abstract

A compact Energy Recovery Linac (cERL) is under construction at KEK in order to test the performance of the key components required for the future ERL project. The main linac L-band cavities were assembled and tested in the cryomodule under high power operation. During the test, information concerning field emission were gathered by using PIN diodes rings and NaI scintillator located at the cavities ends. With Si PIN diodes, it is possible to observe the radiation pattern produced by field emission, inferring the meridian where the emitter belongs. On the other hand, the bremsstrahlung spectra recorded with the scintillator allow estimation of the longitudinal emitter location. The data were analyzed by means of simulations, taking into account the cavities operating conditions and interactions between the accelerated electrons and the cavity surface. The resulting information are used to monitor the cavity performance and to deduce a possible emitter location.

### INTRODUCTION

A compact Energy Recovery Linac (cERL) is under construction at KEK in order to proof the performance of the key components required for the future ERL project [1], in figure 1 is shown a schematic view for cERL. Two L-band cavities were assembled and tested in the main linac cryomodule under high power operation in December 2012 [2,3].

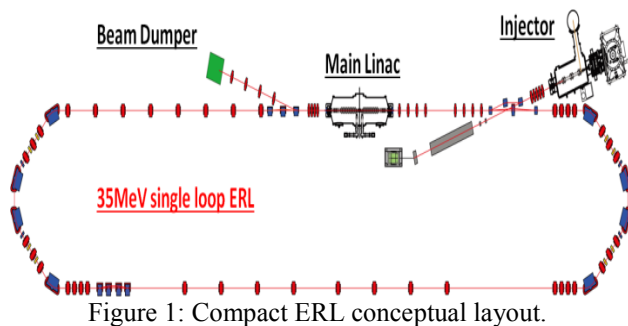


Figure 1: Compact ERL conceptual layout.

### EXPERIMENTAL SETUP

A set of PIN diodes and NaI scintillator were installed inside and around the cryomodule in order to detect radiation pattern and its intensity during operation. The radiation can be produced by field emitted electrons, which are accelerated inside the cavity and injected to the cavity surface or to the gate valves located at cryomodule ends.

<sup>#</sup>enrico@post.kek.jp

**Si PIN Diodes:** Sets of ring shape 16 PIN diodes were installed at four locations near the cavities as shown in figure 2. For each cavity, a first set of PIN diode ring was positioned between the eccentric fluted pipes and the helium jacket (SBP3, SBP4), and a second set of ring was installed on the taper beam pipe located after the cavity large beam pipe (LBP3, LBP4). The diodes signal reveals the radiation angular pattern if any field emission occurs during cavity operation.

**NaI Scintillator:** The detector was placed near the cryomodule, as shown in figure 2, behind a lead shield with a collimator window (2x2mm) on the beam axis. The scintillator crystal was a 2"x2" inches, and connected to a photomultiplier and a multichannel analyzer. Before the test, the detector was calibrated by means of known radioactive sources ( $\text{Na}_{22}$ ,  $\text{Co}_{60}$  and  $\text{Cs}_{137}$ ). The radiation background was measured for 1 hour before each test. The bremsstrahlung radiation produced by emitted electrons incident to the gate valve is recorded in order to reveal the longitudinal emitter position. By knowing the electrons kinetic energy and the cavity accelerating field, it is possible to determine from which irises the electrons were originated.

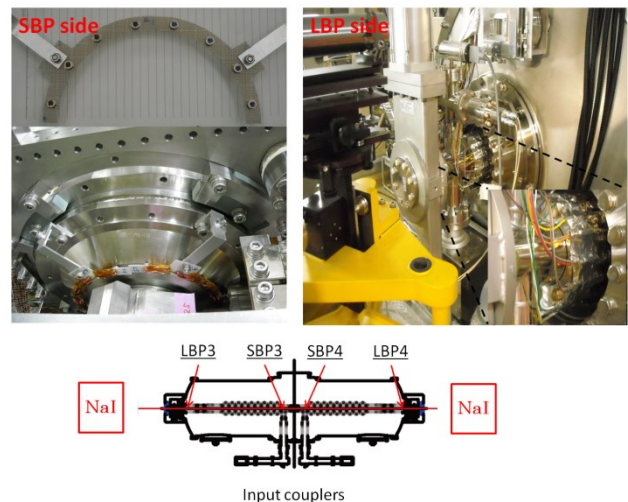


Figure 2: PIN diodes setup (above) and cryomodule top view with PIN diodes and scintillator location (below).

The two cavities installed in the cryomodule are identified as “upstream cavity (#4)” for the one near the injector, and as “downstream cavity (#3)” for the one near the beam dumper.

### EXPERIMENTAL RESULTS

After cool down to 2K, the cavities were tested one by one. During the test, the cavity voltage ( $V_c$ ) was progressively increased and the PIN diodes signals were continuously recorded. The data acquisition for the diodes signal was performed by a customized EPICS. The NaI scintillator data were recorded by the PC connected to the multichannel analyzer.

**Upstream Cavity (#4):** Radiation was first detected when the cavity voltage was about 8 MV. As can be seen in figure 3, a peak in PIN diodes signal was detected in the upper part on the LBP side.

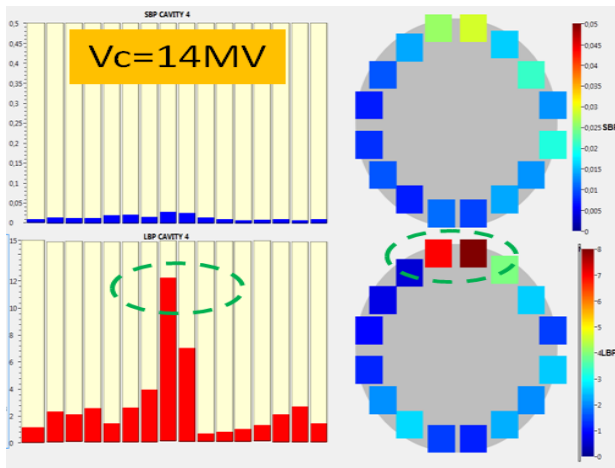


Figure 3: PIN diodes signal from upstream cavity (cavity #4) with  $V_c=14$ MV, SBP side (above) and LBP side (below). Data were recorded before burst event.

While keeping the cavity voltage at 14 MV, a radiation burst occurred. After this event, the radiation pattern changed as shown in figure 4.

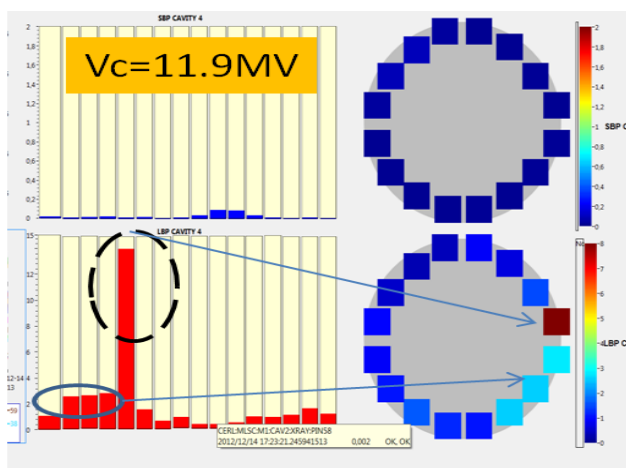


Figure 4: PIN diodes signal from upstream cavity (cavity #4) with  $V_c=11.9$ MV, SBP side (above) and LBP side (below). Data were recorded after burst event.

A new emitter appeared on the horizontal meridian ( $90^\circ$ ). The signal peak was located on the right part on the LBP side.

### 05 Cavity performance limiting mechanisms

#### R. Field emission & multipacting

**Downstream Cavity (#3):** Radiation started to be detected when the cavity voltage was about 7 MV. As shown in figure 5, a peak in the PIN diodes signal was located around  $45^\circ$  meridian on the LBP side.

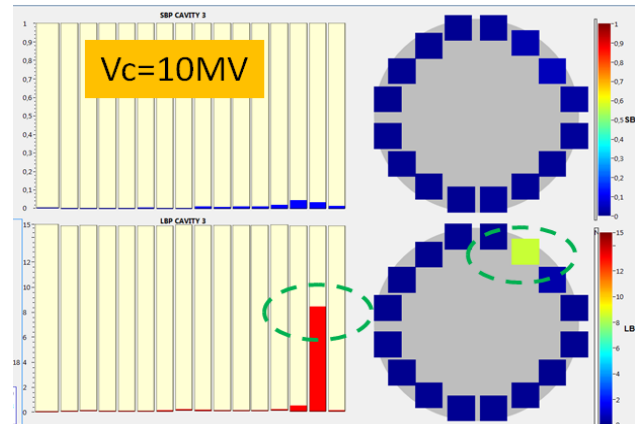


Figure 5: PIN diodes signal from downstream cavity (cavity #3) with  $V_c=10$ MV, SBP side (above) and LBP side (below).

**NaI Scintillator:** The bremsstrahlung radiation spectra were measured for both cavities near the field emission onset. During the measurement, the scintillator was located in front of the gate valve, as shown in figure 2. The cavity voltage was kept stable during the data acquisition of 2 minutes. The background signal was subtracted and the data were binned by dividing the energy interval in 200 KeV step. The measurement results corresponding to the upstream and downstream cavities are shown on figures 6 and 7. Each measurement was performed at different cavity voltages, from 8 MV to 9.5 MV for the upstream cavity, and from 7MV to 8.5 MV for the downstream cavity. The data for upstream cavity (#4) were taken after burst event.

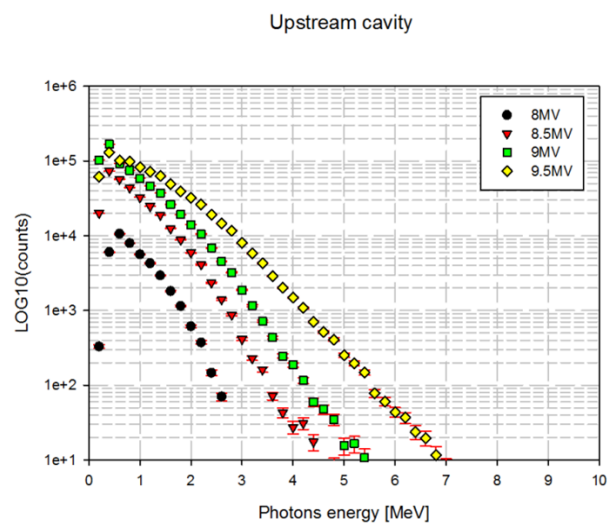


Figure 6: Bremsstrahlung radiation at different cavity voltage (upstream cavity).

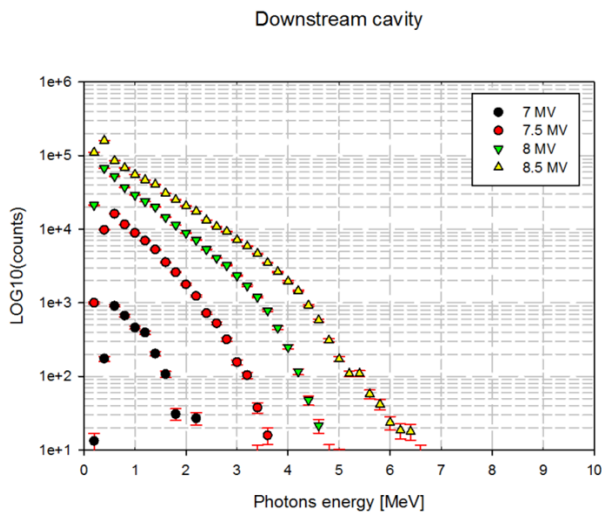


Figure 7: Bremsstrahlung radiation at different cavity voltage (downstream cavity).

**Radiation Onset:** Radiation monitors were placed on both sides of cryomodule near the cavity axis. It was possible to measure the radiation dose at different cavity voltage as shown in figure 8 [2].

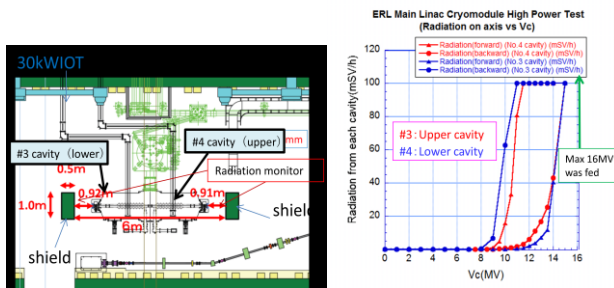


Figure 8: (Left) setup of the high power test of cERL main-linac cryomodule. (Right) Measured accelerating voltage ( $V_c$ ) and radiation doses for both cavities.

## DISCUSSION

### Comparison with Vertical Test Results

It is possible to compare the cavity performance during the high power test with the one at their previous vertical test. Both cavities showed a performance degradation since their last vertical test, as indicated the following aspects.

**Quality Factor  $Q_0$ :** The unloaded Q exceeded the design requirement during their last vertical test as shown in figure 9 and figure 10 [4].

At the high power test, the unloaded Q dropped drastically due to strong field emission.

**Field Emission Onset:** As shown in table 1, the field emission onsets were decreased compared to the last vertical test for both cavities.

**Radiation Pattern:** during the high power test, the radiation pattern was detected by Si PIN diodes installed at cavity ends. The value of the meridian angle where radiation was detected during vertical test and high power test is reported in table 2.

Table 1: Field Emission Onset

Cavity #	Field emission onset [MV/m]	
	Vertical test	High power test
Upstream (#4)	22	8
Downstream (#3)	13	7

Upstream cavity (#4)

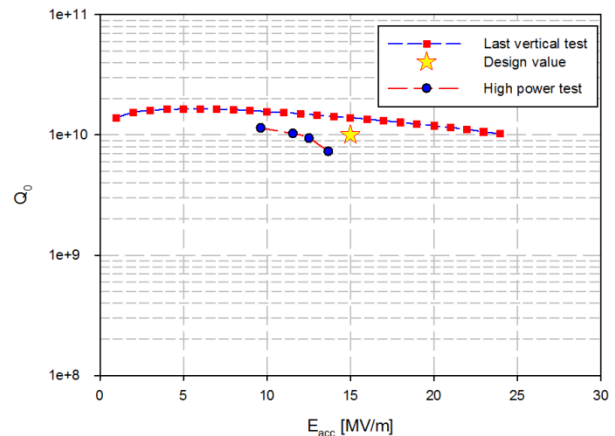


Figure 9: Q-E plot for upstream cavity (#4) during the last vertical test (red squares) and high power test (blue dots).

Downstream cavity (#3)

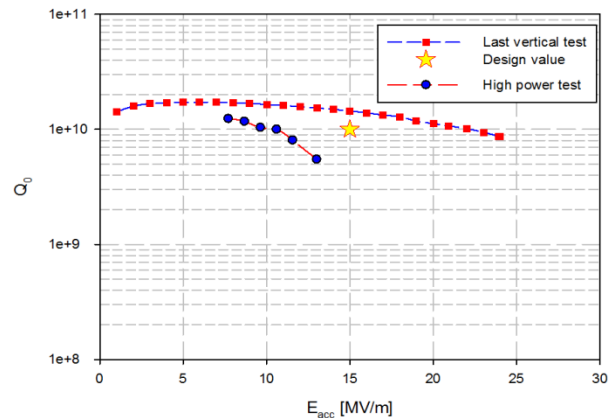


Figure 10: Q-E plot for downstream cavity (#3) during the last vertical test (red squares) and high power test (blue dots).

Table 2: Radiation Meridian Angle

Cavity #	Meridian angle	
	Vertical test	High power test
Upstream (#4) before burst	45°	0°
Upstream (#4) after burst		90°
Downstream (#3)	112°	45°

The meridian angle, where radiation was detected, varied in both cases. From the data collected, it seems that new emitters were introduced on the cavity surface during the cavities installation into cryomodule. The

origin of the emitters is not yet clear, but the changes in the cavity performance and radiation pattern strongly suggest the appearance of new field emission sources.

**Emitter Location**

We estimated the emitter location by using experimental data and simulation results.

First, we extrapolated the electron maximum kinetic energy from the scintillator data. Through a fitting in the middle section of each curve (linear part), it was possible to calculate the maximum kinetic energy at each cavity field. The calculated maximum kinetic energy with respect to each cavity accelerating field is presented in table 3. The conversion between the cavity voltage and the accelerating field was performed through the equation  $V_c[\text{MV}] = 1.038 \times E_{\text{acc}}[\text{MV/m}]$ , where 1.038 is the cavity length in meter,  $V_c$  is the cavity accelerating voltage and  $E_{\text{acc}}$  is the accelerating gradient.

Table 3: Estimated Electron Maximum Kinetic Energy

$V_c$ [MV]	$E_{\text{acc}}$ [MV/m]	Maximum kinetic energy [MeV]	
		Upstream (#4)	Downstream (#3)
7	6.7	--	3.0
7.5	7.2	--	4.5
8	7.7	4.0	5.6
8.5	8.2	5.5	7.2
9	8.7	6.4	--
9.5	9.2	8.5	--

Next, we estimated the relation between emitter location and electron kinetic energy using simulation code. The FishPact code [5] is used for this purpose. The electron trajectories originated from an emitter located on the iris between the 1<sup>st</sup> and 2<sup>nd</sup> cell are depicted on figure 11. Each trajectory starts at different RF phases and lands at a different location on the cavity surface [6].

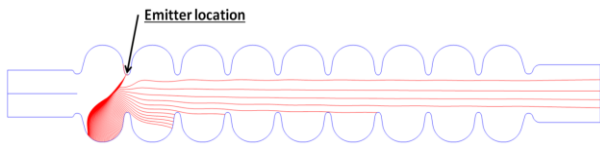


Figure 11: Electron trajectories at different RF phase originated by emitter located on iris between 1<sup>st</sup> and 2<sup>nd</sup> cell,  $E_{\text{acc}} = 15 \text{ MV/m}$ .

Figure 12 presents the maximum kinetic energy for electrons landing on right end (LBP side). For the simulation, only electrons that land in a 1 cm radius around the beam axis were recorded to take into account the effect of collimator window. Electrons were generated from emitters on different iris along a 3 cm line and spaced by 0.5 mm.

Comparing the scintillator data and the simulation results, it seems that for both cavities emitters were located in the first two cells. Indeed the emitter in the downstream cavity (#3) it probably located in the 1<sup>st</sup> cell, and the emitter in upstream (#4) cavity in the 2<sup>nd</sup> cell.

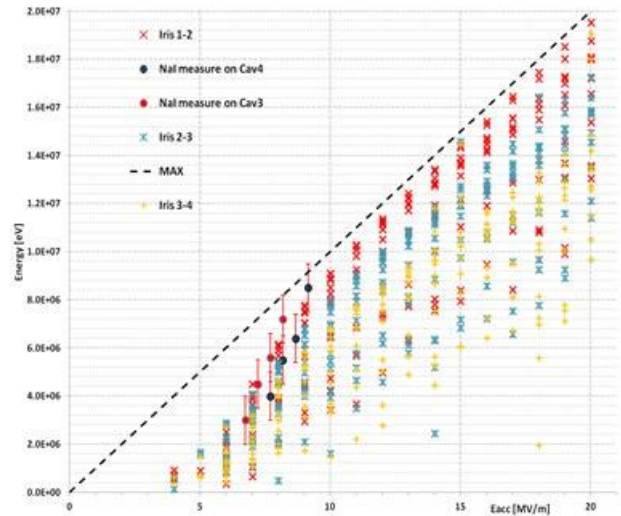


Figure 12: Electron maximum kinetic energy, from emitters on 1<sup>st</sup> cell iris (red cross), on 2<sup>nd</sup> cell (blue cross) and 3<sup>rd</sup> cell (yellow cross). Electron energy extrapolated from scintillator data from upstream cavity (dark blue dots) and downstream cavity (red dots).

Furthermore, it was possible to narrow the probable origin region by considering the relation between the emitter location and the landing location at different RF phases. Figure 13 and figure 14 show the electrons landing location with respect to the emitter position and RF phase during emission at 8.5 MV cavity voltage is 8.5 MV (figure 13 for emitters on the iris between 2<sup>nd</sup> and 3<sup>rd</sup> cell, figure 14 for emitters on the iris between 1<sup>st</sup> and 2<sup>nd</sup> cell). The black dots represent electron trajectories that can reach the LBP side. The region that can emit electrons towards the LBP side extends for about 7 mm along the iris.

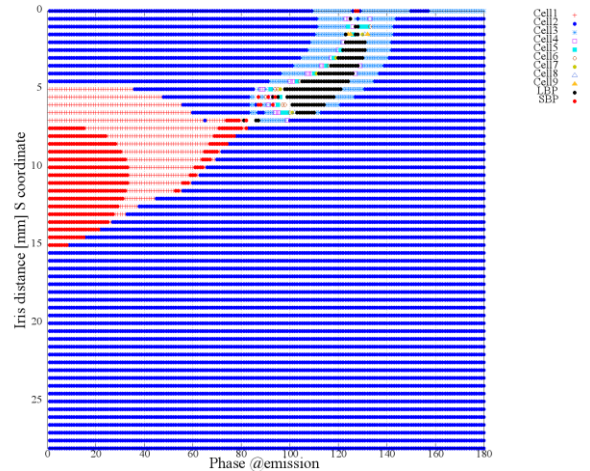


Figure 13: Electrons landing location with respect to RF phase during emission and emitter position (distance from iris). Emitters are located along the iris in 2<sup>nd</sup> cell.

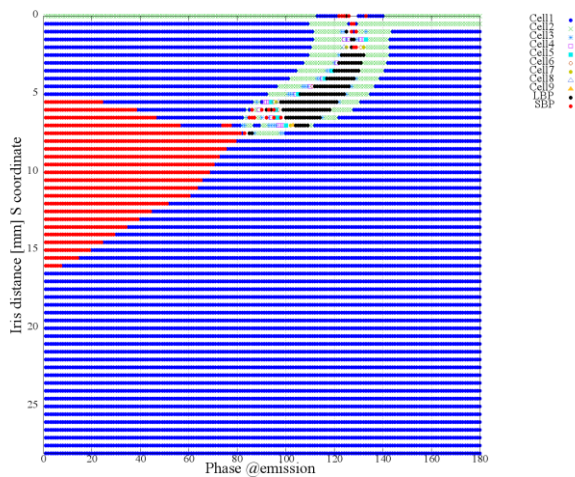


Figure 14: Electrons landing location with respect to RF phase during emission and emitter position (distance from iris). Emitters are located along the iris in 1st cell.

By considering the information gathered through the PIN diodes and NaI scintillator it was possible to identify a probable emitter location in each cavity, which are displayed on figure 15. The region where the emitter can be located has some square centimetre extension, taking into account the uncertainty due to the finite PIN diodes number (that defines the meridian) and the length along the iris surface (as shown in figure 13 and 14).

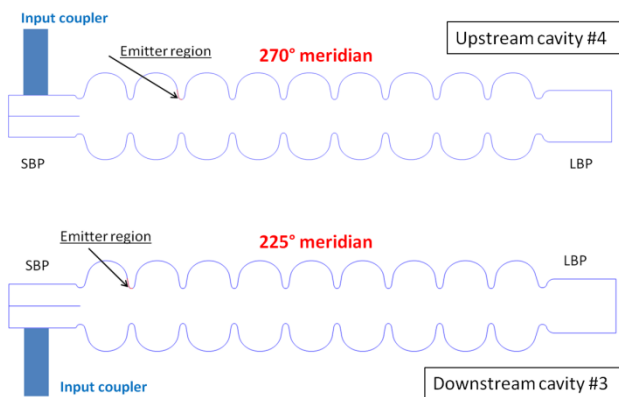


Figure 15: Emitter area location for upstream (above) and downstream (below) cavity.

The emitter region is located on the iris surface facing the SBP side on the opposite meridian with respect to radiation peak. This choice come from an extensive analysis performed on radiation patterns recorded during vertical tests [6,7]. By taking into account the electron trajectories, their kinetic energy and the emitted current it was possible to determine the radiation peaks.

## SUMMARY

The main linac cavities were assembled in the cryomodule and tested in high power regime. PIN diodes sensors and NaI scintillator were installed around the cryomodule in order to detect the radiation produced by field emitted electrons. Performance degradation was

observed for both cavities compared to the results obtained during their last vertical test. A different radiation pattern was observed along with a lower field emission onset. Probably during the assembly operation new emitters landed on the cavity surface. Through the data gathered with PIN diodes and scintillator and also using simulation results, it was possible to define an area where most probably the emitters were located.

## REFERENCES

- [1] S. Sakanaka *et al.*, “Progress in Construction of the 35MeV Compact Energy Recovery Linac at KEK”, IPAC’13.
- [2] H. Sakai *et al.*, “High power CW tests of cERL main-linac cryomodule”, *these proceedings*.
- [3] K. Umemori *et al.*, “Design of L-band superconducting cavity for the energy recovery linacs”, APAC’07.
- [4] K. Umemori *et al.*, “Vertical test results for ERL 9-cell cavities for compact ERL project”, IPAC’12.
- [5] <http://code.google.com/p/fishpack/>
- [6] E. Cenni *et al.*, “Field emission simulation for KEK-ERL 9cell superconducting cavity”, IPAC’12.
- [7] E. Cenni, PhD dissertation (to be published).